Shock-Fitting Solution of the Supersonic Flowfield in a Rounded Internal Corner

James A. Martin*
NASA Langley Research Center, Hampton, Virginia

The conical inviscid supersonic flowfield in a rounded internal corner was investigated numerically. A number of comparisons were made with previously obtained sharp corner solutions, and an experiment was conducted to provide a rounded corner comparison. The experimental investigation included mapping of the shock wave and contact surface locations at a Mach number of 4.1 for a model with unequal wedge angles and a conically rounded corner. There is little pressure change across the three-dimensional flowfield with a sharp corner. As the amount of corner rounding is increased, the pressure gradient toward the corner increases, and pockets of increased pressure appear at the ends of the rounded section. Increasing the freestream Mach number changes the relative shock-wave shapes. The solution was successfully executed over a range of Mach numbers from 2 to 6 and over a range of wedge angles from 4 to 18 deg.

Nomenclature

a = speed of sound
$a_{11},\ldots,a_{48}$ = coefficients of transformed equations
C_V = specific heat at constant volume
E = Euler solution
F = freestream in triple-point solution
I = intermediate shock wave, region between the intermediate shock wave and the contact surface in triple-point solution
M = Mach number
N = new solution
p = pressure
P = natural logarithm of pressure
Q = any quantity to be integrated
R = gas constant, region between the reflected shock wave and the constant surface in triple-point solution
Ry,Rz = reflected shock waves ending at the surface near the y and z axes, respectively
s = surface
S = entropy
t = total
T = temperature
u,v,w = velocity components in the x, y, and z directions, respectively
V = velocity
$(\;)_w$ = wedge
W = wedge flow region in triple-point solution
x,y,z = Cartesian coordinates
y_{ws} = wedge shock-wave location
$\Delta\alpha$ = small downstream angle change in triple-point solution
β,ϕ,ψ = computational coordinates
γ = ratio of specific heats
ξ,η,ζ = rotated Cartesian coordinates
θ = shock-wave angle
ν = flow angle
ρ = density
σ,τ = velocity angularities, $v/x, w/x$
$(\_)_\infty$ = freestream quantity
$(\underline{\underline{\;}})$ = vector quantity
$(\bar{\;})$ = prediction step in integration

Introduction

RECENT developments of supersonic combustion ramjets (scramjets) have concentrated on the use of vehicle-integrated inlets as shown on Fig. 1 to gain the maximum benefit from the compressive flowfield generated by the vehicle.[1] Modular engines with rectangular inlets have several advantages in vehicle-integrated designs, including the easier development of modules compared with complete systems.

The performance predicted for vehicle-integrated scramjets is good, but the estimated structural mass of these engines is high. Although this mass may be acceptable for many applications, it represents a significant penalty when the scramjet is applied to a system that is mass sensitive such as a single-stage Earth-to-orbit vehicle. Vehicle studies[2] indicate that if the scramjet mass can be reduced significantly, there is a substantial advantage to be gained by using the scramjet on Earth-to-orbit vehicles. One way to reduce the scramjet mass is to use a circular cross section in the combustor, where maintaining a rectangular cross section causes a large structural penalty because of the high internal pressure. One estimate[3] shows that the engine mass may be reduced up to 40% with a circular, as opposed to a rectangular, cross section in the combustor.

A scramjet with a circular cross section in the combustor and a rectangular cross section in the front of the inlet includes an inlet flowfield that is neither rectangular nor axisymmetric. As a first step toward the understanding of such inlets, the conical supersonic flowfield in a rounded internal corner was investigated.

A second purpose of the current research was to develop a shock-fitting scheme for flowfield solutions in a manner that may be more easily understood and applied to a variety of problems. There are several differences between the current formulation and previous shock-fitting solutions. In each instance, the current approach is oriented toward a physical understanding of the phenomena, a minimum of complexity in derivation of the needed equations and program logic, and minimization of computer storage. The resulting computer program can be operated in an interactive mode on an economical minicomputer. This approach minimizes the time

---

Presented as Paper 83-0038 at the AIAA 21st Aerospace Sciences Meeting, Reno, Nev., Jan. 11-13, 1983; received Feb. 9, 1983; revision received April 24, 1984. This paper is declared a work of the U.S. Government and therefore is in the public domain.

*Aerospace Engineer, Space System Division. Senior Member AIAA.

to develop new solutions and the chance for errors that would be difficult to detect.

Corner Flows

The inviscid flowfield that exists near the intersection of two wedges in a supersonic freestream flow is illustrated in Fig. 2. Each wedge deflects the freestream flow and creates a wedge shock wave and a two-dimensional wedge flow. Near the corner created by the intersection of the wedges, there is a three-dimensional interaction. An intermediate shock wave lies between the two wedge shock waves, and two reflected shock waves lie between the body surface and the intersections of the wedge shock waves with the intermediate shock wave. The intersections of the wedge shock wave, the intermediate shock wave, and the reflected shock wave are called triple points. Triple points occur along two lines starting at the corner along the leading edge and extending along both sides of the intermediate shock wave. The reflected shock waves meet the body surface at shock-surface intersection points.

An inviscid corner flow can be conical; that is, the flow conditions are constant along any ray starting at the corner along the leading edge. Conical flow occurs whenever there is no characteristic length with which to form dimensionless lengths so that all characteristics of the flowfield depend only on angles about some point. The entire flowfield can, therefore, be represented by the flowfield at a plane normal to the freestream at any distance downstream of the leading edge. Figure 3 shows the flowfield at a plane; such views are usually displayed looking downstream.

Between the lines of triple points and the corner are two contact surfaces which appear as dashed lines in Fig. 3. The flow enclosed by the two contact surfaces and the intermediate shock wave is relatively high-entropy flow that has passed through the intermediate shock wave, which is stronger than the wedge or reflected shock waves. The two triangles bounded by the contact surfaces, the reflected shock waves, and the body surface contain lower entropy flow. This lower entropy flow has passed sequentially through a wedge shock wave and a reflected shock wave.

The boundary layers can transmit information from the three-dimensional flow near the corner into the wedge flow. At low Reynolds numbers, there can be significant interactions between the boundary layers and the reflected shock waves. Computational solutions for these cases are possible for low Reynolds numbers, but become increasingly difficult as the Reynolds number increases. At high Reynolds numbers typical of flight applications, the importance of boundary-layer interactions is decreased so that inviscid solutions are useful. For inviscid solutions, there is no mechanism for transmitting information beyond the intermediate and reflected shock waves, so the three-dimensional effects caused by the corner are limited to the flow enclosed by the intermediate and reflected shock waves and by the body surface.

Several previous investigations of corner flows have been reported, both experimental[4-8] and numerical.[9-12] Kutler[13] and others[14-16] solved the inviscid compressive corner flow problem using a shock-capturing technique. In this scheme, the governing equations are written in conservative form so that integration can proceed through shock waves. By computing the flowfield over a region extending beyond the reflected and intermediate shock waves, the location of the shock waves appears as jumps in pressure or other quantities which are not conserved. Inviscid corner-flow solutions have been obtained by Marconi[17] and Salas[18] using the shock-fitting method. In this scheme, the locations of the shock waves are an integral part of the solution, and the Rankine-Hugoniot conditions are used to calculate the jumps across them. This method has the potential for solving a flowfield with fewer computational mesh points than the shock-capturing method, since the definition depends on the mesh spacing only along the shock wave.

The difference in geometry of the body surface between the current solution and previous solutions is the addition of a curved section or fillet in the corner. The radius of the curved section is proportional to the downstream dimension, thereby maintaining conical flow. The center of curvature is located such that the curved section is tangent to both wedge surfaces.

Analytical Approach and Development

A finite difference, shock-fitting approach was selected for this analysis. The solution was marched downstream to convergence. The contact surfaces in the flowfield were not fitted, so the entropy was integrated using windward differences. At the surface, a method using an isentropic turn to correct the flow direction was used. At the shock waves, an extension of this approach was devised to allow a turn of the internal flow and an adjustment of the shock-wave slope to satisfy both pressure and velocity direction constraints. Some aspects of the development are discussed subsequently and a more complete discussion is given in Ref. 19.

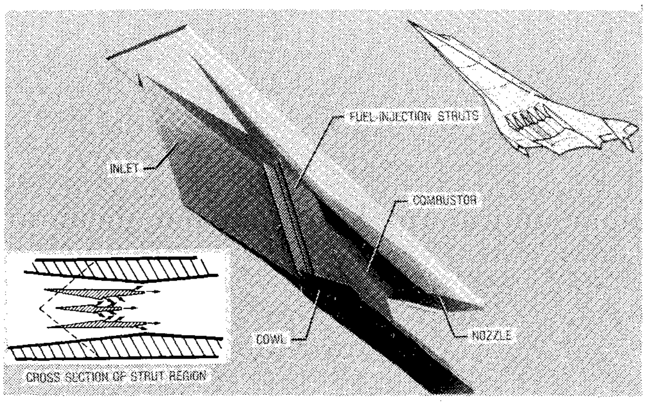

Fig. 1 Airframe-integrated supersonic combustion ramjet.

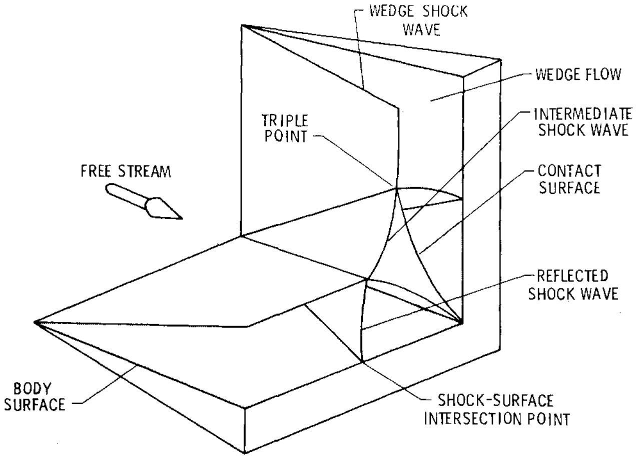

Fig. 2 Corner flow.

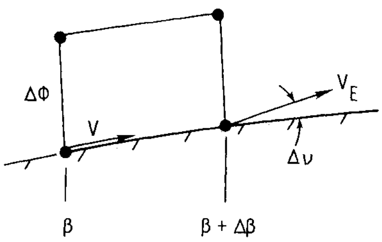

Fig. 3 Surface calculation.

Governing Equations

In this section, the governing equations are developed in a form suitable for finite difference, downstream-marching integration in a shock-fitting scheme. The steps include nondimensionalization, elimination of the density, formation of the velocity angularities, and separation of the downstream derivatives.

Consider a rectangular, Cartesian coordinate system. The governing equations for inviscid, steady-state flow are put in dimensionless form by defining dimensionless quantities as follows: pressure, density, and temperature divided by freestream values; velocities divided by $\sqrt{p_\infty/\rho_\infty}$; and entropy by subtracting the freestream entropy and dividing the difference by C_V. In the dimensionless form, R does not appear.

The entropy relationship requires integration, and substituting for the temperature from the equation of state and combining the density terms gives

$$S = \ell n p - \gamma \ell n \rho \tag{1}$$

For computational purposes, the use of the natural logarithm of the pressure P is preferred (rather than the absolute pressure) in order to get stable numerical results over a wide range of pressures.

The elimination of the density from the equations by using the pressure and entropy is also desirable. The pressure is more useful for visualizing flow changes, and one variable can be eliminated. Although T will appear in the resulting equations, it will be found from Eq. (1) with the equation of state.

The next step is to introduce the velocity angularities to allow integration across the contact surfaces. The velocity components can be integrated satisfactorily in most of the flowfield, but there are contact surfaces across which the velocity components can have a discontinuity. The angularities can be integrated across the contact surfaces, since the flow is parallel to these surfaces.

The integration procedure requires solving for the x derivatives. The pressure equation can be written:

$$P_x = -\frac{\sigma P_y - \tau P_z - \gamma(\sigma_y + \tau_z)}{(u^2/\gamma T) - 1}\,\frac{u^2}{\gamma T} \tag{2}$$

The denominator is the square of a Mach number based on the downstream velocity component minus one. The solution can only be calculated if the downstream Mach number at all points remains sufficiently greater than one to avoid numerical difficulties. This condition is expected physically, since steady supersonic flow can be calculated by downstream marching schemes and steady subsonic flow cannot.

With P_x known, the other equations can be written

$$\sigma_x = -\sigma\sigma_y - \tau\sigma_z - (T/u^2)(P_y - \sigma P_x) \tag{3}$$

$$\tau_x = -\sigma\tau_y - \tau\tau_z - (T/u^2)(P_z - \tau P_x) \tag{4}$$

$$S_x = -\sigma S_y - \tau S_z \tag{5}$$

Integration of Eqs. (2-5) will give P, σ, τ, and S at a new point. Since the five quantities P, u, v, w, and S must be known at the new point, another relation is needed. The flowfield being considered is adiabatic; thus, the total temperature will remain constant at the freestream value $T_{t,\infty}$, and the total-temperature equation can be solved for the velocity magnitude. The velocity components may then be obtained using the velocity magnitude relation.

Coordinate Mapping

The region over which the equations are to be solved is mapped such that it becomes a rectangle. The sides of the rectangle are the surface, the reflected shock waves, and the intermediate shock wave (I). A single mapping such as one involving

$$\phi = (y - y_s)/(y_I - y_s) \tag{6}$$

would probably cause problems since a line of constant ϕ could have the same y value on s and I. The denominator would then be zero. To avoid this, a preliminary mapping

$$\xi = x \qquad \eta = (y+z)/\sqrt{2} \qquad \zeta = (z-y)/\sqrt{2} \tag{7}$$

is used to rotate the region $\pi/4$.

The mapping of computational coordinates is, then,

$$\beta = \xi \qquad \phi = \frac{\eta - \eta_s}{\eta_I - \eta_s} \qquad \psi = \frac{\zeta - \zeta_{RY}}{\zeta_{Rz} - \zeta_{Ry}} \tag{8}$$

Care must be taken at this point to clarify the meaning of η_s, η_I, ζ_{Ry}, and ζ_{Rz}. At a given value of ψ, increasing ϕ implies moving along a curved line from the surface (at η_s) to the intermediate shock wave (at η_I). The values of η_I and η_s to be used in evaluating ϕ in Eq. (8) should be the same along that constant-ψ line. Derivatives of ϕ will involve derivatives of η_s and η_I, and these derivatives should be evaluated at points along the boundaries corresponding to the same ψ value at the point where the derivative is desired.

The approach taken here could be described as an explicit formulation of the transformation. Derivatives of the boundary locations, such as $\partial\eta_I/\partial\zeta$, will be found in terms of the physical coordinates. Therefore, the derivatives of the

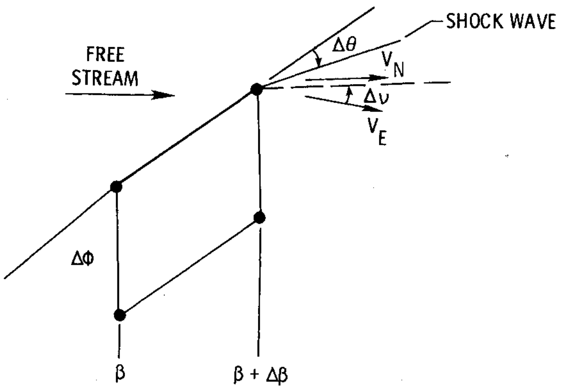

Fig. 4 Shock-wave calculation.

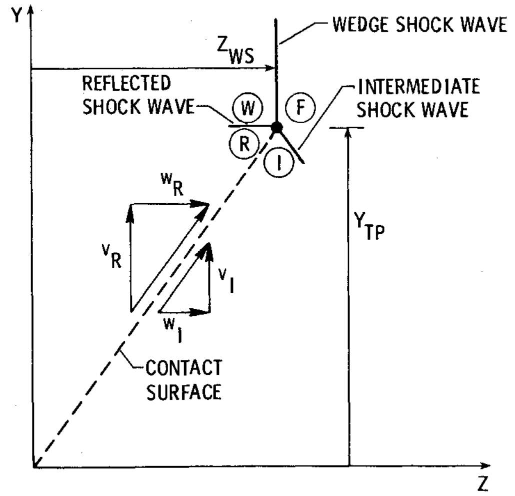

Fig. 5 Nomenclature near a triple point and velocity vector components near a contact surface.

computational coordinates in terms of the physical coordinates, such as $\partial\phi/\partial\zeta$, are given explicitly. In previous shock-fitting solutions, an implicit formulation has been used. If the location of the boundaries is stored in terms of the computational coordinates and derivatives of the boundaries are found only in terms of the computational coordinates, a set of linear equations results which must be solved. For the current problem, the algebra of the implicit formulation was quite complex, and the resulting equations were difficult to understand physically. Also, the derivatives of the boundaries have less physical meaning in terms of computational coordinates than in terms of physical coordinates.

The transformation of the governing equations from the physical to the computational plane is found by applying the chain rule. The derivatives are given explicitly. Knowing the necessary derivatives, the governing equations can be written in computational coordinates and the values of the coefficients are given in Ref. 19.

Integration at the Surface

Along the surface, the normal integration scheme must be modified because the boundary condition of flow tangent to the surface must be satisfied. An approach proposed by Abbett[20] was adopted. This scheme, illustrated in Fig. 4, uses an estimate of the flowfield on the surface at $\beta+\Delta\beta$ based on integration of the Euler equations. In general, the Euler velocity V_E is not tangent to the surface, and the flow is turned based on a Prandtl-Meyer turn to satisfy the boundary condition.

Integration at Shock Waves

In marching the solution downstream, a new location of the shock wave and a new shock-wave normal which defines the shock-wave slope are estimated. Figure 5 illustrates the geometry for the intermediate shock wave. All variables, including the shock-wave normal, are known on the β plane. Integration of the Euler equations using information at β provides information from the internal flowfield to the shock-wave point at $\beta+\Delta\beta$. The resulting flow conditions are represented by $\tilde{V}_E$.

Because the flow at $\beta+\Delta\beta$ has a pressure and velocity direction different from those at β, the shock-wave slope must change by some angle $\Delta\theta$. Many schemes assume that the shock wave changes such that the pressure downstream of the modified shock wave is equal to the pressure given by the Euler integration of the flowfield. This is not exactly correct. The disturbance from the Euler integration interacts with the shock wave, and a new disturbance is reflected from the shock wave. The flow $\tilde{V}_E$ is, therefore, turned some angle $\Delta\nu$. The shock-wave slope and the turning angle $\Delta\nu$ must have values that allow the pressure and velocity direction along the resulting contact surface to be equal. There are, therefore, two conditions for two unknowns.

The solution scheme that is used starts with the location of the shock wave at $\beta+\Delta\beta$. For this the slope $\partial\eta_I/\partial\beta$ at β is used. Using the new shock-wave locations, η_I at $(\xi+\Delta\xi, \zeta\pm\Delta\zeta)$, the slope of the shock wave in the ξ plane, $\partial\eta_I/\partial\zeta$, can be found. The slope $\partial\eta_I/\partial\xi$ at $\beta+\Delta\beta$ will be found iteratively. The initial estimate will be the value at β. With values for $\partial\eta_I/\partial\xi$ and $\partial\eta_I/\partial\zeta$, the new shock-wave normal can be found, and the new flow conditions can be determined.

A Prandtl-Meyer turn is applied to the flow such that the pressure equals P_N, found from the new shock-wave solution just stated. To first order, the change in flow direction needed to equalize the pressure is

$$\Delta\nu_P = \frac{1-e^{P_N-P_E}}{\gamma M_E^2} \tag{9}$$

Changing the internal flow to equalize pressure results in an overlap of the flows which can be estimated. This overlap (angle) is an indicator of the change in the shock-wave slope that is needed to satisfy both pressure and velocity direction. Only part of this turn should be applied to the shock wave, since a change in the shock wave is accompanied by a change in the turning angle. The turning angle is added directly to the shock-wave slope $\partial\eta_I/\partial\xi$. The value of $\partial\eta_I/\partial\zeta$ is retained, since the location of the shock-wave points is not changed. The process is repeated until the overlap is insignificant. The flow conditions at the point are taken from the Rankine-Hugoniot relations for the final shock-wave slope.

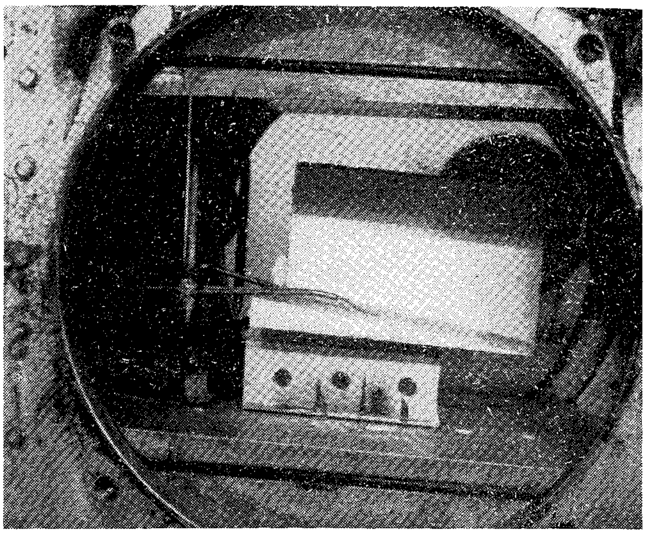

Fig. 6 Experimental model installation.

Intersections of Shock Waves with Surfaces

Normally, the downstream slope of a shock wave is used to predict the location of the shock wave for the next downstream step. At the surface intersection, the slope along the shock wave in the next plane is also known from the normality condition. The shock-wave location at the surface was found by using the location of the adjacent point and this slope.

Triple Points

The geometry of the triple point near the y wedge is shown in Fig. 5 for one x location. The triple point is located on the wedge shock wave, so the z dimension is z_{ws}, and z_{ws}/x is constant. The y dimension is denoted y_{TP}, and it must be assumed for the starting conditions. The marching scheme adjusts y_{TP} until a solution is achieved. When the conical solution is achieved, y_{TP}/x is constant.

Figure 5 also shows the notation for the regions at the triple point. The freestream is region F, and the wedge flow region W. The region between the reflected shock wave and the contact surface is region R, and the region between the intermediate shock wave and the contact surface is region I. The flow conditions in regions F and W are known from initial conditions and the wedge flow solution.

The slopes of the reflected and intermediate shock waves along the shock waves in Fig. 5 are found from numerical differencing of the locations as at other shock-wave points. The downstream slopes of the shock waves are adjusted to satisfy the two flow conditions along the contact surface. The first condition is that P_R and P_I be equal. The second condition is that $\tilde{V}_R$ and $\tilde{V}_I$ are parallel to the contact surface. This will be true if the triangles of Fig. 5 are similar.

The adjustments can be estimated by solving simultaneous linear equations for the Taylor series expansions. A small angle change, $\Delta\alpha$, in the downstream slopes produces perturbed values when the oblique shock-wave calculations are made with and without $\Delta\alpha$. The coefficients in the series are the numerical-difference approximations to the derivatives of the conditions with respect to α.

Integration

The MacCormack second-order integration scheme[21] was used. The scheme has been a popular one and has been shown to work well for similar problems. The two-step difference method for any quantity Q is defined by

$$\tilde{\tilde{Q}}(x+\Delta x,y,z)=Q(x,y,z)+Q_x(x,y,z)\Delta x \tag{10}$$

$$Q(x+\Delta x,y,z)=\tfrac{1}{2}[Q(x,y,z)+\tilde{\tilde{Q}}(x+\Delta x,y,z)+\tilde{\tilde{Q}}_x(x+\Delta x,y,z)\Delta x] \tag{11}$$

where $\tilde{\tilde{Q}}(x+\Delta x,y,z)$ is a prediction of $Q(x+\Delta x,y,z)$ that is improved in the corrector step, and $\tilde{\tilde{Q}}_x(x+\Delta x,y,z)$ is a derivative in the marching direction based on predicted values.

The derivatives in the marching direction, such as $Q_x(x,y,z)$, are given by the governing equations in terms of the derivatives in the current plane, such as $Q_y(x,y,z)$. The derivatives in the current plane are found by one-sided differences such as

$$Q_y(x,y,z)=[Q(x,y+\Delta y,z)-Q(x,y,z)]/\Delta y \tag{12}$$

In this scheme, forward differences ($\Delta y>0$) are used in the predictor step to get $\tilde{\tilde{Q}}(x+\Delta x,y,z)$. In the corrector step, backward differences are used ($\Delta y<0$) to get $\tilde{\tilde{Q}}_x(x+\Delta x,y,z)$ so that the result is balanced.

Damping

When the solution is calculated without damping, oscillations can appear which are not physically meaningful.[22] These oscillations are usually spaced such that a parameter such as pressure is high at one grid point and low at adjacent grid points. In the downstream direction, the oscillations can exist for several hundred steps with little change. In order to smooth these oscillations, damping is applied. A fourth-order damping is used so that the damping does not affect the solution in any way other than to damp the oscillations. The form of the damping is

$$\Delta Q=-c[Q(y-2\Delta y)+(y+2\Delta y)-4Q(y-\Delta y)-4Q(y+\Delta y)+6Q(y)] \tag{13}$$

Damping is applied to the integrated variables p, σ, and τ in both the ϕ and ψ coordinates and to the shock-wave locations along the shock waves after completing each downstream step. Typical values of the damping coefficient are 0.001 to 0.01.

Experimental Investigation

An experimental investigation was conducted in order to verify the validity of the computational results. Results of previous analyses and experimental investigations were available to verify the results with no corner rounding, but no results were found in a literature survey which could be used to compare the calculated effects of the corner with rounding. The facility[23] used was a continuous-flow dry-air wind tunnel with a Mach number of approximately 4.1 and a square test section with 0.23-m sides. The tunnel exhausted to the atmosphere and utilized two-dimensional fixed geometry nozzle blocks and a secondary minimum followed by a subsonic diffuser. The Reynolds number, based on test-section conditions upstream of the model and the model length, was 13×10^6 with a total temperature of 289 K and a total pressure of 1.38 MPa.

The model, shown in Fig. 6, was constructed of aluminum with sharp leading edges and wedge angles of 6 and 4 deg. The length was 203 mm, the height and width were both 127 mm, and the radius of the corner divided by the downstream location is constant at 0.0893. The resulting thicknesses of the wedges at the aft end of the model were 21 mm for the 6-deg wedge and 14 mm for the 4-deg wedge. The model was mounted to the floor of the facility. Because of inaccuracies in the mounting and bending of the mount during initial runs, the actual angles of the wedge surfaces to the axis of the facility were 8.00 and 5.43 deg for the wedges along the y and z axes, respectively.

Although the model did not occupy a large fraction of the cross-sectional area of the facility, starting the wind tunnel was a significant problem. This was because the model was not symmetric and the mounting was made of thick aluminum angle stock with large bolts and nuts. Initially, a large probe with several Pitot tubes was tried, but hard tunnel starts in this mode caused the bending of the model mounting. This problem was alleviated by installation of a single Pitot probe.

The probe shown in Fig. 6 was used to measure Pitot pressure at a plane near the midpoint of the model in the downstream direction. The tip diameter of the probe was 1.5 mm. Most of the measurements were made with a shorter probe ending at the aft end of the model. The probe was manually placed at a lateral position before each run and was driven vertically during each run. The Pitot pressure was continuously measured. A change in the measured pressure indicated that the probe was crossing a shock wave or contact surface, and the position of the probe at that time determined the location of the disturbance. Figure 7 shows a typical complete Pitot-pressure trace. The boundary layer, contact surfaces, and shock waves are noted.

An initial group of runs was made with the probe placed first near the corner and then moved outward during each run. Additional runs were then made in locations that would provide more data near the triple points, including runs that were essentially repeats of previous locations. All of these runs are included in the computation of the data, and the scatter of the data indicates to some extent the accuracy of the results.

Figure 8 shows the primary results of the experimental investigation. The figure is shown from the aft of the model looking upstream. The freestream flow is in the portion of the figure farthest from the corner, beyond the data points. The nearly two-dimensional wedge shock waves extend upward and to the right in the figure. Between each of these shock waves and the wedge surfaces, the flow is nearly a two-dimensional wedge flow. The wedge shock waves do not intersect each other; there is an intermediate shock wave formed (also shown on Fig. 2).

At each of the intersections of the wedge shock waves and the intermediate shock wave, two discontinuities are formed. One is a reflected shock wave which extends toward the surface. The other is a contact surface which extends toward

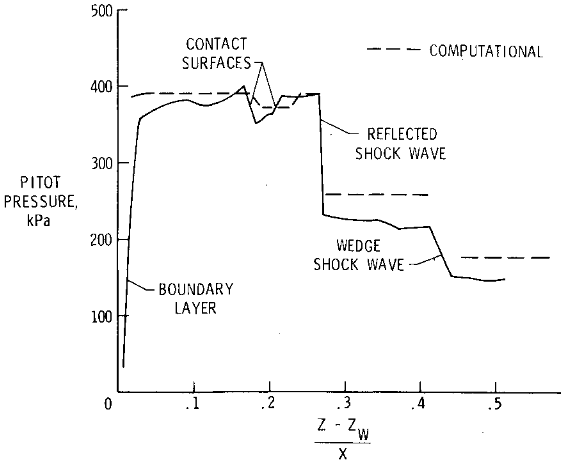

Fig. 7 Typical complete Pitot-pressure trace. $(y-y_w)/x$ of 0.197-0.217. Computational solution includes a boundary-layer displacement.

the corner. The contact surface separates the flow which came through the intermediate shock wave from the flow which came through both the wedge and reflected shock waves. The two points where the wedge shock waves, intermediate shock waves, and reflected shock waves intersect are called triple points. The intermediate shock wave was relatively short.

Because the experimental model was finite in height and width, edges of the model influenced a portion of the flow. Figure 9 shows an estimate of the extent of these portions of the flow at the aft end of the model. These portions of the flow are conical, with the vertex of each cone at the leading edge of a wedge at the end farthest from the corner. These portions of the flow do not include the triple points or contact surfaces at the aft end of the model, and they include less of the flowfield on the forward portion of the model. Therefore, the results of the experimental investigation should be useful to compare to an analytical solution that assumes infinite wedges as long as the data points in the influenced portions of the flow are not included in the comparisons. In order to enhance the understanding of the experimental data, extensions of the wedge shock waves were added in Fig. 14 where they would theoretically appear if the model were infinite in height and width.

Two additional areas of concern exist for the use of the experimental data in evaluating the analysis. One involves viscous effects and the boundary layer on the model. The pressure-probe data indicated that the boundary-layer thickness at the aft end of the model was approximately 8 mm. This effect is evaluated in the Results section. The second difference is the angularity of the freestream flow with respect to the facility axis. Unpublished surveys of the facility indicate that this angularity is within one degree in the region of the model; therefore, the effects on the results should be minimal.

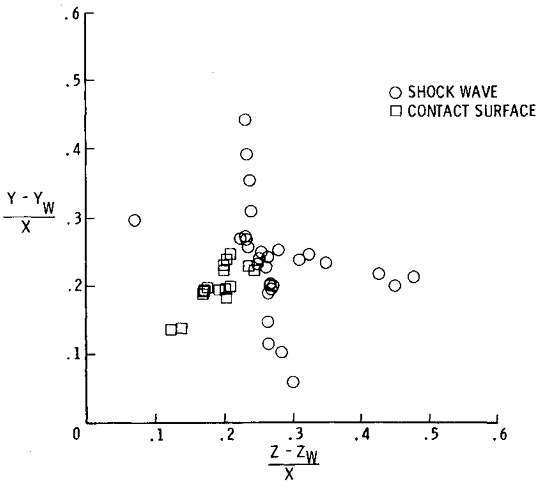

Fig. 8 Overall experimental results; $M_\infty = 4.1$, $\delta = 8.00$ and 5.43, and $R/x = 0.0893$.

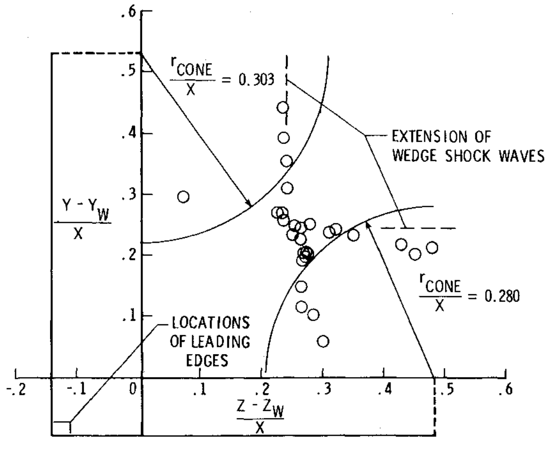

Fig. 9 Region of edge effects for experimental data; $M_\infty = 4.1$, $\delta = 8.00$ and 5.43, and $R/x = 0.0893$.

Results

Comparisons between the current results and two previous analytical solutions for cases with symmetric wedges and no corner rounding are shown in Fig. 10. The results of Kutler[13]

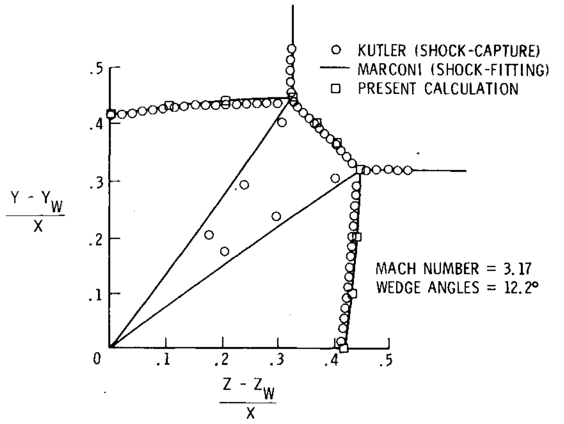

Fig. 10 Comparisons of shock-wave locations with previous results for a sharp corner; $M_\infty = 3.17$, $\delta = 12.2$, $R/x = 0$, and 28×28 grid.

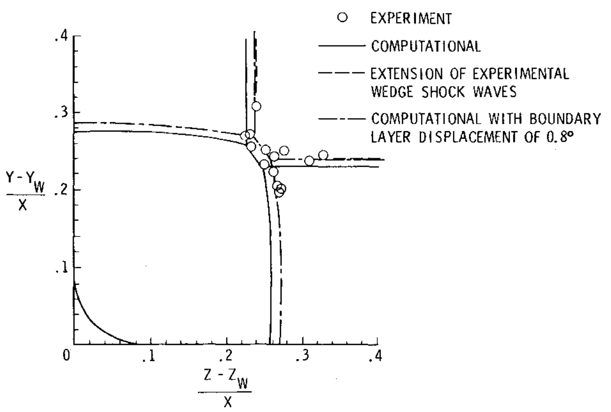

Fig. 11 Effect of boundary-layer displacement on comparisons of computational and experimental shock-wave locations; $M_\infty = 4.1$, $\delta = 8.00$ and 5.43, $R/x = 0.0893$, and 28×28 grid.

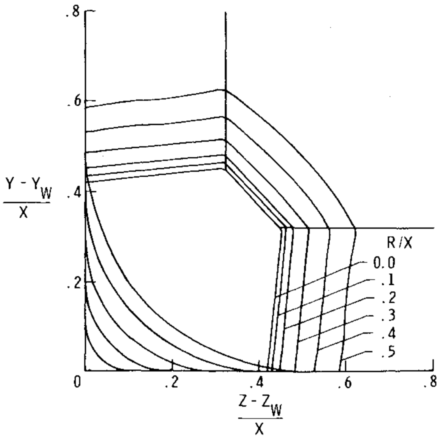

Fig. 12 Effect of rounding on shock-wave locations; $M_\infty = 3.17$, $\delta = 12.2$, and 28×28 grid.

were obtained using a shock-capturing technique. The results of Marconi[17] were obtained using a shock-fitting technique similar to the current results. The agreement between the three different methods shown indicates that the methods give similar solutions even with different approaches.

A comparison between the current computational results and the experimental results for a rounded corner is shown in Fig. 11. In general, the experimental results indicate shock-wave locations farther from the surface than do the computational results. This is expected because of the displacement effect of the boundary layer on the experimental results. The inviscid results do not account for the boundary-layer effects. The computational solution depends on the wedge shock-wave locations. The difference in the computational and experimental wedge shock-wave locations are therefore an indication of the expected difference in the intermediate shock-wave locations.

Figure 11 also shows how the inclusion of a boundary-layer displacement affects the computational solution. The experimental data indicated a boundary-layer thickness of 8 mm at the aft end of the model on the 8-deg wedge. Assuming a laminar boundary layer and using Blasius laminar boundary-layer theory to get a ratio of the displacement thickness to the boundary-layer thickness, a value of 3 mm was calculated for the displacement thickness. The displacement thickness is the required body surface change for an inviscid solution to simulate a viscous flow, since it accounts for the mass-flow deficiency due to the viscous effects. The 3-mm displacement thickness corresponds to an angular displacement of 0.8 deg; therefore, the computational solution was repeated with the wedge angles each increased by 0.8 deg. The results indicate that most of the differences between the computational and experimental results are due to the boundary-layer displacement.

A comparison between the experimental results and the computational results with the displacement thickness added to the wedges is also shown in Fig. 7. The Pitot pressure is compared along a typical pass of the experimental probe. The experimental results for $(z-z_w)/x$ greater than 0.3 do not agree well with the computational results, which is expected because of the edge effects on the experimental results. The results in the three-dimensional-flow zone (inside the reflected shock wave) agree reasonably well. The experimental results show the expected effect of the boundary layer near the surface and also show other variations that do not appear in the computational solution. These variations could be a result of the curvature and transitional state of the boundary layer.

One parametric effect that was investigated was the effect of rounding in the corner. Figure 12 shows several effects on the shock-wave shapes that result from increasing R/x from 0.0 to 0.5. The triple points move out along the wedge shock waves, which increases the length of the intermediate shock waves. The intersections of the reflected shock waves with the surface move away from the corner nearly the same amount that the triple points move along the wedge shock waves. As a result, the reflected shock waves are nearly parallel. There is a slight convex shape to the intermediate shock waves that becomes more obvious as the length increases. The reflected shock waves remain fairly straight except near the triple point.

Figure 13 shows pressure contours for R/x of 0.5. Without rounding, the pressure increases slightly from the shock waves to the corner with some higher pressures near the triple points. As the rounding is increased, the pressure gradient from the intermediate shock wave toward the corner increases significantly. In terms of potential vehicle applications, this indicates a more severe environment for the vehicle structure in a rounded corner than in a sharp corner with the same wedge angles. At the higher values of R/x, there are noticeable pockets of increased pressure at each end of the rounded section, and the pressure at the center of the rounded section is lower than at the ends. The pockets of increased pressure are a result of the change in curvature of the surface at the ends of the rounded section. The pressure on the straight sections of the surface increases from the reflected shock wave to the rounded section.

Figure 14 shows the region over which execution of the program has been successful for symmetric wedge angles and sharp corners. There is a region at low-wedge angles where the triple points merge. The program does not execute in this region, but three-dimensional solutions are not needed in this region. There is a region at low-freestream Mach numbers and high-wedge angles that results in a subsonic downstream component of the flow behind the intermediate shock wave. The program cannot operate in this region because the governing equations contain a denominator that is zero when the downstream component of the velocity is sonic. At freestream Mach numbers of 5-6 and wedge angles of 8 deg or less, the damping had to be increased to achieve solutions. Solutions were obtained with R/x of 0.2 over a similar region.

Most solutions were obtained using approximate initial conditions based on straight shock waves, and grid refinement also was utilized. Near the subsonic flow boundary, this approach did not work because subsonic flow occurred at intermediate steps. The restart capability developed for the computer program was used in these cases; a successful solution was used as input for a case with a lower freestream Mach number or a higher wedge angle. As the boundary was approached, the changes that could be accepted grew smaller. For example, at a freestream Mach number of 3.17, the solution for wedge angles of 16 deg was used as input to generate a solution for wedge angles of 18 deg. Using the solution at 18 deg as input, a solution was generated at 19 deg, but a solution at 20 deg could not be achieved.

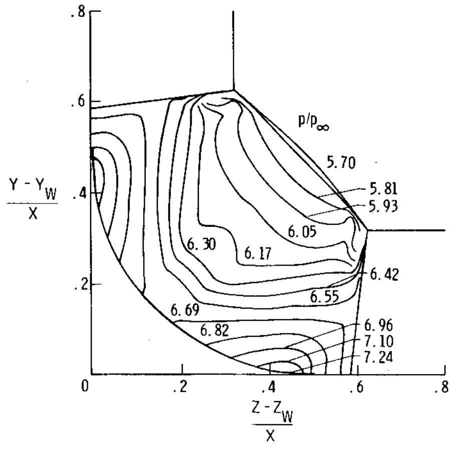

Fig. 13 Shock-wave locations and pressure contours; $M_\infty = 3.17$, $\delta = 12.2$, $R/x = 0.5$, and 28×28 grid.

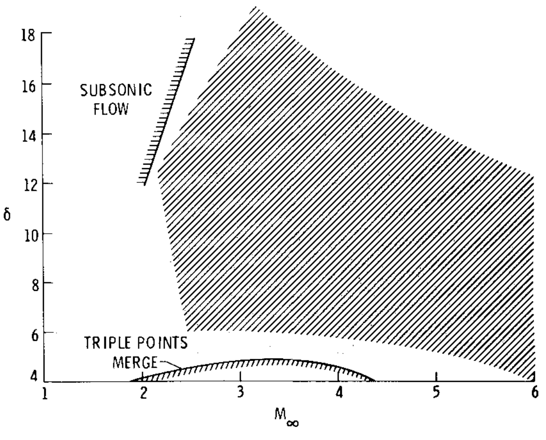

Fig. 14 Region of successful convergence; $R/x = 0$ and 28×28 grid.

Concluding Remarks

The flowfield created by supersonic flow over an internal corner with rounding was investigated numerically. Experimental results were obtained at a freestream Mach number of 4.1 for comparison with the computational results.

The computational investigations utilized a shock-fitting, finite difference scheme. An explicit formulation of the transformation to computational coordinates was used. The contact surfaces were not fitted. The surface boundary conditions were satisfied by turning the flow isentropically after each integration step. The shock waves were turned at each integration step such that both pressure and flow angularity conditions were satisfied. The schemes chosen, compared to previous shock-fitting solutions, minimize the algebraic manipulations required to derive the equations needed for the solution and maximize the use of physically understandable phenomena such as isentropic turns. The computational solution utilized a computer program with several useful features.

Solutions calculated with the computer program agreed with previous solutions for the sharp-corner case and with the experimental investigation results for the rounded-corner case. The computations converge rapidly to the solution. Parametric effects were computed for variations in corner rounding, freestream Mach number, and symmetric and unsymmetric wedge angles. A region was described where successful executions were obtained.

In addition to the understanding of corner flows provided by the solutions presented, the results of this investigation have several potential applications. The computer program can be used in the current form to calculate the flow in the four corners of an inlet until the point at which interactions between the corners begin. With some modification, the computer program might be used to calculate the flow in corners that are not conical. In this case, a conical solution would be generated first and used as a starting point to march downstream. The modifications to the existing program would mostly be limited to the surface geometry subroutine. A solution from the current program can also be used as a starting point for a more general marching solution of an entire inlet. In a more general sense, several techniques developed in this investigation could be used in solutions for supersonic flow past other types of bodies.

References

[1] Jones, R. A. and Huber, P. W., "Airframe-Integrated Propulsion System for Hypersonic Cruise Vehicles," presented at the 11th Congress of the ICAS, Lisbon, Portugal, Sept. 1978.

[2] Martin, J. A., "Ramjet Propulsion for Single-Stage-to-Orbit Vehicles," *Journal of Spacecraft and Rockets*, Vol. 15, Sept. 1978, pp. 259-260.

[3] Jackson, L. R., Martin, J. A., and Small, W. J., "A Fully Reusable, Horizontal Takeoff Space Transport Concept with Two Small Turbo-jet Boosters," NASA TM-74087, Oct. 1977.

[4] Charwat, A. F. and Redekeopp, L. G., "Supersonic Interference Flow Along the Corner of Intersecting Wedges," *AIAA Journal*, Vol. 5, March 1967.

[5] Stainbeck, P. C. and Weinstein, L. M., "Corner Flow at Hypersonic Speeds," NASA SP-148, May 1967.

[6] Cresci, R. J., Rubin, S. G., and Nardo, C. J., "Hypersonic Flow in Rectangular and Non-Rectangular Corners," *Hypersonic Boundary Layers and Flow Fields*, AGARD CF 30, May 1968.

[7] West, J. E. and Korkegi, R. H., "Supersonic Interaction in the Corner of Intersecting Wedges at High Reynolds Numbers," *AIAA Journal*, Vol. 10, May 1972, pp. 652-656.

[8] Nangia, R. K., "Three-Dimensional Wave Interactions in Supersonic Intakes," presented at the 2nd International Symposium on Air Breathing Engines, March 1974.

[9] Korkegi, R. H., "Limit Case for Supersonic Inviscid Flow in the Corner of Intersecting Wedges," *AIAA Journal*, Vol. 7, March 1969, pp. 569-570.

[10] Shang, J. W. and Hankey, W. L., "Numerical Solution of the Compressible Navier-Stokes Equations for a Three-Dimensional Corner," AIAA Paper 77-169, 1977.

[11] Smith, R. E., "Numerical Solution of the Navier-Stokes Equations for a Family of Three-Dimensional Corner Geometries," AIAA Paper 80-1349, July 1980.

[12] Goebel, T. P., "A Theoretical Study of Inviscid, Supersonic Flow Along a Corner Formed by the Intersection of Two Wedges," Ph.D. Dissertation, University of California, Los Angeles, Calif., 1969.

[13] Kutler, P., "Numerical Solution for the Inviscid Supersonic Flow in the Corner Formed by Two Intersecting Wedges," AIAA Paper 73-675, July 1973.

[14] Shankar, V., Anderson, D., and Kutler, P., "Numerical Solutions for Supersonic Corner Flow," *Journal of Computational Physics*, Vol. 17, Feb. 1975, pp. 160-179.

[15] Kutler, P., Shankar, V., Anderson, D. A., and Sorenson, R. L., "Internal and External Axial Corner Flows," NASA SP-347, March 1975.

[16] Anderson, D. A. and Nangia, R. K., "Comparison of Numerical and Experimental "Conical" Flow Fields in Supersonic Corners with Compression and/or Expansion," *The Aeronautical Quarterly*, Vol. 28, Nov. 1977, pp. 293-306.

[17] Marconi, F., "Internal Corner Flow Fields," AIAA Paper 79-0014, Jan. 1979.

[18] Salas, M. D., "Careful Numerical Study of Flowfields About Asymmetric External Conical Corners," AIAA Paper 79-1511, July 1979.

[19] Martin, J. A., "The Supersonic Flowfield in a Rounded Internal Corner," D.Sc. Dissertation, George Washington University, Washington, D.C., Nov. 1981.

[20] Abbett, M. J., "Boundary Condition Computational Procedures for Inviscid, Supersonic Steady Flow Field Calculations," Aerotherm Report 71-41, Mountain View, Calif., Nov. 1971.

[21] MacCormack, R. W., "The Effect of Viscosity in Hypervelocity Impact Cratering," AIAA Paper 69-354, May 1969.

[22] Barnwell, R. B., "A Time-Dependent Method for Calculating Supersonic Blunt-Body Flow Fields with Sharp Corners and Embedded Shock Waves," NASA TN D-6031, Nov. 1970.

[23] Torrence, M. G., "Concentration Measurements of an Injected Gas in a Supersonic Stream," NASA TN D-3860, April 1967.